

# Chapter 4

## Jet Formation at the Spill Site and Resulting Droplet Size Distributions



Karen Malone, Zachary M. Aman, Simeon Pesch, Michael Schlüter,  
and Dieter Krause

**Abstract** The size distribution of oil droplets and gas bubbles forming at the exit geometry of a deep-sea blowout is one of the key parameters to understand its propagation and fate in the ocean, whether with regard to rising time to the surface, drift by ocean currents, dissolution or biodegradation. While a large 8 mm droplet might rise to the sea surface within minutes or hours, microdroplets  $<100\ \mu\text{m}$  may take weeks or months to surface, if at all. On the other hand, a microdroplet or bubble dissolves faster due to its larger surface to volume ratio and is also more available for biodegrading bacteria. To be able to properly model these effects, it is necessary to understand the drop formation processes near the discharge point and to predict the evolving droplet size distribution (DSD) for the specific conditions.

In this chapter, the general breakup mechanisms and flow regimes of an oil-in-water jet are discussed in Sect. 4.1. Section 4.2 focuses on the different approaches to determine the DSD in the laboratory and field settings and critically reviews the existing datasets. State-of-the-art models for the prediction of the DSD of a subsea oil discharge are presented alongside a new approach based on the turbulent kinetic energy (TKE) in Sect. 4.3, while Sect. 4.4 takes a closer look at the specific effects of the deep sea on the DSD. Based on this, Sect. 4.5 discusses the advantages and limitations of subsea dispersant injection. Section 4.6 provides a summary of the chapter and gives an outlook to unresolved questions.

---

K. Malone (✉) · D. Krause  
Hamburg University of Technology, Institute of Product Development and Mechanical  
Engineering Design, Hamburg, Germany  
e-mail: [karen.malone@tuhh.de](mailto:karen.malone@tuhh.de); [krause@tuhh.de](mailto:krause@tuhh.de)

Z. M. Aman  
University of Western Australia, Department of Chemical Engineering, Perth, WA, Australia  
e-mail: [zachary.aman@uwa.edu.au](mailto:zachary.aman@uwa.edu.au)

S. Pesch · M. Schlüter  
Hamburg University of Technology, Institute of Multiphase Flows, Hamburg, Germany  
e-mail: [simeon.pesch@tuhh.de](mailto:simeon.pesch@tuhh.de); [michael.schluter@tuhh.de](mailto:michael.schluter@tuhh.de)

**Keywords** Jet formation · Droplet size distribution · Live oil · Median drop size · Flow regime · Turbulent kinetic energy · Turbulence · Droplet breakup · Near-field · In situ measurements · Dissolved gas · Outgassing · Phase change · Dispersants

## Nomenclature

### *Latin*

$A$	Empirical coefficient in the modified Weber number scaling
$B$	Empirical coefficient in the modified Weber number scaling
CDF	Cumulative distribution function
$D$	Nozzle/discharge diameter
$d_{32}$	Sauter diameter
$d_{n50}$	Median diameter of number distribution
$d_p$	Drop/particle diameter
$d_{v50}$	Median diameter of volume distribution
DOR	Dispersant-to-oil ratio
DSD	Drop size distribution
$\text{erf}(x)$	Gauss error function
$\text{exp}(x)$	Exponential function
IFT	Interfacial tension
$k_i$	Scaling factor
$M$	Oil mass inside the nozzle
Oh	Ohnesorge number
$p$	Pressure
$\Delta p$	Pressure drop at the nozzle
$Q$	Volume flow rate
$Re$	Reynolds number
$u_1$	Exit velocity of dispersed liquid phase
$\nu_i$	Viscosity number
We	Weber number
$We^*$	Modified Weber number

### *Greek*

$\alpha$	Spreading factor of the Rosin-Rammler distribution function
$\varepsilon$	Turbulent energy dissipation rate
$\varepsilon_u$	Turbulent energy dissipation rate caused by the exit velocity
$\varepsilon_{pd}$	Turbulent energy dissipation rate caused by pressure drop at the nozzle
$\eta_l$	Dynamic viscosity of dispersed liquid phase
$\rho_l$	Density of dispersed liquid phase
$\rho_c$	Density of continuous phase
$\sigma$	Spreading factor of the log-normal distribution function
$\sigma_l$	Interfacial tension (IFT) between dispersed liquid phase and continuous phase

## 4.1 Introduction

When crude oil enters into seawater from a pipeline or a well, drop formation will occur in different ways based on the characteristics of the discharge. In general, oil drop formation is governed by the relation of stabilizing forces (interfacial tension, viscosity) versus destabilizing forces such as turbulence within the oil and the water phase, friction and cavitation (Lefebvre and McDonell 2017). There are several studies distinguishing a number of different flow regimes, ranging from the formation of single drops at the exit geometry to full atomization of a jet (Masutani and Adams 2001; Boxall et al. 2012; Ohnesorge 1936; Lefebvre and McDonell 2017).

Originally, Ohnesorge (1936) identified four different regimes (see Fig. 4.1):

0. Formation of individual drops at the nozzle without jet formation.
- I. Breakup of a cylindrical jet caused by Rayleigh instability.
- II. Breakup caused by sinuous waves along the jet.
- III. Atomization of the jet due to turbulent breakup.

The different regimes are distinguished using the relation between the dimensionless Reynolds number ( $Re$ )

$$Re = \frac{D \cdot \rho_1 \cdot u_1}{\eta_1} \quad (4.1)$$

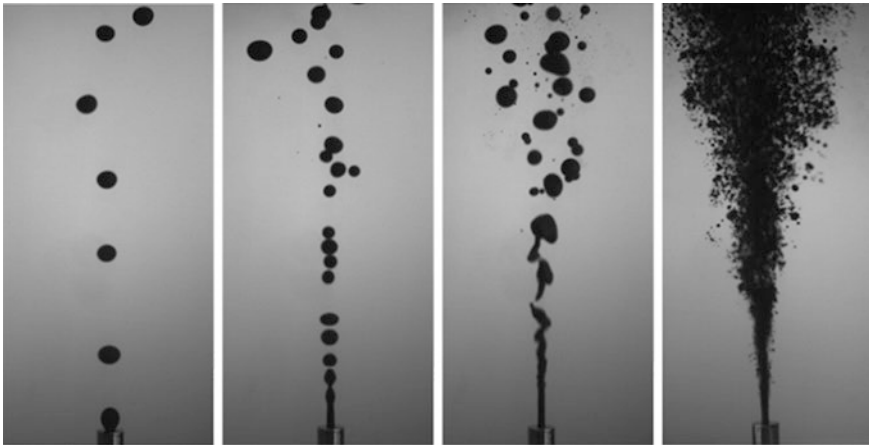


**Fig. 4.1** Different breakup/flow regimes of Louisiana sweet crude oil discharged into artificial seawater at 150 bar, 20 °C from a 1.5 mm nozzle. Volume flow increases from left to right. Far left: regime (0), individual drop formation. Mid left: regime (I), Rayleigh instability. Mid right: regime (II), sinuous wave breakup. Far right: regime (III), atomization, turbulent breakup

and Ohnesorge number (Oh)

$$\text{Oh} = \frac{\eta_i}{D \cdot \rho_i \cdot \sigma_i} \quad (4.2)$$

with  $D$  as the discharge diameter,  $\rho_i$  is the oil density,  $\sigma_i$  is the oil-water interfacial tension (IFT),  $\eta_i$  is the dynamic viscosity of the oil and  $u_i$  is the oil exit velocity at the nozzle. In each regime, the breakup of the dispersed oil into drops is governed by different mechanisms. While the drop diameter is mainly determined by the exit geometry, buoyancy and interfacial tension between oil and water in regime (0), the atomization regime is mainly governed by turbulence and the shear forces acting between oil and water. Since the original work of Ohnesorge, several authors have sought to specify the borders of these and additional sub-regimes (e.g. Tang 2004; Hsiang and Faeth 1992; Masutani and Adams 2001; Adams and Socolofsky 2004; Lefebvre and McDonnell 2017), especially with regard to the transition from Rayleigh instability to full atomization. In a major oil well blowout, it can, however, be assumed that the discharged liquid will be well beyond the atomization boarder (Masutani and Adams 2001). In the following therefore only the drop formation processes in a fully atomized jet will be considered. As it represents the upper limit of the different approaches for classification of the flow regimes, Tang's expression (Tang 2004)

$$\text{Oh} \geq 24.9548 \cdot Re^{-1.0027} \quad (4.3)$$

is chosen to mark the transition to full atomization and turbulent breakup.

The breakup of a turbulent jet consists of two phases, the primary and secondary breakup. In the primary breakup, ligaments form at the edge of the cylindrical jet due to shear between the continuous phase and the jet, which eventually break up into drops. The secondary breakup describes the further disintegration of these initial drops into smaller drops due to the ambient flow field. The primary breakup stage has a major influence on the final droplet size distribution (DSD) and is mainly controlled by the discharge conditions at the nozzle (Lefebvre and McDonnell 2017). The hydrodynamics taking place at this stage of the jet formation are very complex and not yet fully understood (Zuzio et al. 2013).

As a result of the turbulent nature of an atomized jet, the formation and size of individual drops cannot be predicted. The entirety of all drops in an atomized jet can, however, approximately be described using a characteristic average diameter and a size distribution function. Depending on the area of application, different characteristic diameters are used. In oil spill modelling, the median diameters of the number ( $d_{n50}$ ) or volume distribution ( $d_{v50}$ ) are most commonly used, describing the 50th percentile of all drops by number and total oil volume, respectively. With regard to mass transfer between the dispersed and the continuous phase, the Sauter mean diameter ( $d_{32}$ ) has been established. It describes a drop with the same volume to surface ratio as the overall oil phase and can be calculated using:

$$d_{32} = \frac{\sum_{i=1}^n d_i^3}{\sum_{i=1}^n d_i^2} \quad (4.4)$$

The DSD of a dispersed oil phase is widely discussed in the literature. Experimental studies mostly found either a Rosin-Rammler distribution (e.g. Johansen et al. 2013) according to

$$\text{CDF}(d) = 1 - \exp\left(-k_i \left(\frac{d}{d_i}\right)^\alpha\right) \quad (4.5)$$

or a log-normal distribution function (e.g. Malone et al. 2018)

$$\text{CDF}(d) = \frac{1}{2} + \frac{1}{2} \cdot \text{erf}\left(\frac{\ln d - \ln d_i}{\sqrt{2} \cdot \sigma}\right) \quad (4.6)$$

with  $d_i$  as median diameter,  $\alpha$  and  $\sigma$  spreading coefficients and  $k_i = -\ln(0.5) = 0.69$ . Both functions describe a unimodal size distribution, whereas the Rosin-Rammler distribution is slightly biased towards larger drop diameters in direct comparison of the two.

## 4.2 Determination of Drop Size Distributions in Laboratory and Field Settings

Today, the knowledge on drop formation processes in a subsea oil discharge is based mainly on small-scale experiments in the lab. A single full-scale experiment (“DeepSpill”) has been performed off the Norwegian coast in 2000, and some measurements were taken during the *Deepwater Horizon* (DWH) oil spill in 2010 a large distance from the wellhead.

For a better understanding of the available datasets and the possibilities to assess the DSD experimentally in the lab during a future spill, the different available experimental setups are discussed. Several possibilities for in situ measurements during a spill are presented, and the existing datasets are critically reviewed.

### 4.2.1 Pilot-Scale Jet Experiments

Several studies have been performed to determine drop size distributions from downscaled oil jets entering into seawater at surface conditions, especially since the DWH oil spill. Masutani and Adams (2001) were one of the first to perform in-depth

surveys of the DSD of a vertical oil discharge for several exit velocities and discharge diameters ranging from 1 to 5 mm. A pulse-free gear pump was used to inject the oil from a pressure-free reservoir into a water depth of approximately 1 m. Droplet sizes were determined using a Phase Doppler Particle Analyzer (PDPA). Brandvik et al. (2013) performed a series of experiments using the “Tower Basin” facility at SINTEF, Norway, to measure oil droplet sizes with and without subsea dispersant injection (SSDI). The water tank used was 3 m wide and 6 m deep; oil was injected vertically upward by pressurizing the oil reservoir with nitrogen and releasing the pressurized oil through a controlled valve. Size measurements were taken with both a LISST-100X laser diffractometer and a macro camera 2 m above the nozzle. On the same scale, Belore (2014) investigated the effect of varying dispersant-to-oil ratio (DOR) and gas void fraction on the DSD at Ohmsett Wave Tank. In this study, two LISST-100X laser diffractometers were used to measure the DSD. Zhao et al. (2016) performed experiments at a larger scale also at Ohmsett Wave Tank in 2016 with a discharge of 6.3 L/s from a 1 inch horizontal nozzle; DSD was again determined using two LISST-100X.

These and other similar studies provide key information on the DSD of an oil-only discharge in shallow waters. But because of the limitations of the facilities, the effects of a deep-sea environment such as in the DWH spill could not be investigated. A deep-sea oil discharge will alter from one in shallow waters not only with regard to the water temperature and hydrostatic pressure but also to the high amount of short-chained, gaseous hydrocarbons dissolved in the oil and a pressure difference between the oil reservoir and the surrounding seawater. Recently, two research groups investigated these effects by generating jets under artificial deep-sea conditions. Brandvik et al. (2017) used a holocam (Davies et al. 2017) to determine the DSD of “live oil”, i.e. oil saturated with natural gas, with and without an additional gas void fraction and/or chemical dispersants. The experiments took place in a 2.3-m-wide pressure tank at the Southwest Research Institute (SwRI) at elevated hydrostatic pressures between 59 and 172 bar; jets were generated by overpressure in the oil reservoir. Malone et al. (2018) at Hamburg University of Technology performed several studies at 151 bar hydrostatic pressure to quantify the effects of gas dissolution, outgassing and sudden pressure loss at the nozzle. Oil DSD was determined from an endoscopic imaging system at the centreline of the jet. Oil flow was generated either isobarically or with a defined pressure difference using an equal-volume cylinder (Seemann et al. 2014), enabling a wide range of spill scenarios.

### 4.2.2 *Stirrer Cells*

A different approach to determine the DSD of an accidental oil discharge is based on the turbulent nature of such a discharge. This approach uses a stirrer cell to simulate not the oil jet itself, but rather its turbulent flow field by stirring an oil-in-water

emulsion at a certain speed. This approach avoids upscaling over several orders of magnitude but allows only the investigation of an equilibrated system.

Among others, Boxall et al. (2012) measured the DSD of a water-in-oil emulsion with a combination of the focused beam reflectance method (FBRM) and an endoscopic imaging system for a wide range of oil blends and stirrer speeds. Aman et al. (2015) used the same approach to investigate the DSD under high hydrostatic pressure up to 110 atm in a methane-saturated system using high-speed video image analysis.

### 4.2.3 *DeepSpill: Field Experiment in the Deep Sea*

In June 2000, SINTEF performed a field experiment at the Helland-Hansen site off the coast of Norway in a water depth of 844 m. Four discharges of dyed seawater, crude oil and marine diesel fuel in combination with LNG (liquefied natural gas) or nitrogen were conducted in order to test numerical spill propagation models and equipment for spill monitoring and surveillance (Johansen et al. 2000). The liquids were discharged at a rate of 60 m<sup>3</sup>/h for 60 min each from a 120 mm nozzle; gas flow was between 0.6 and 0.7 Sm<sup>3</sup>/s. Droplet sizes were evaluated manually from ROV video data for one discharge of diesel fuel in combination with LNG at four different heights over the discharge point. Images of the drops were taken by a colour video camera (resolution 460 TV lines) with a ruler mounted in the foreground to provide scale. The reported volume median diameter varies from four distinct values between 3 and 7 mm for the four measurement points ( $d_{v50}$  increasing with increasing distance from the discharge point) (Johansen et al. 2000; Socolofsky et al. 2015) to a single value of 5.5 mm (Brandvik et al. 2017).

### 4.2.4 *Equipment for Field Measurements*

In situ measurement of the DSD of a deep-sea oil spill remains a challenge. Apart from the high-pressure environment, the equipment needs to detect a particle size range of three orders of magnitude, from <10 µm to several millimetres. In addition, the oil fraction in the jet near the discharge point can be very high, resulting in poor light transmittance.

Although originally designed for the quantification of solid particles suspended in the water column, the commercially available LISST laser diffractometers by *Sequoia Scientific Inc.* have been widely used in the past years to measure oil droplet sizes as well (see Sect. 4.2.1). While the system is easy to deploy on ROVs for in situ measurements and also available in a deep-sea configuration (depth rating 3000 m), its measurement range is limited to a maximum drop diameter of 500 µm, a maximum particle concentration of 750 mg/L (less for large particles) and an optical transmission rate >30%. The technology is therefore well suited for

measurements in the far-field plume or intrusion layer but less for determination of the initial DSD next to the discharge site due to the larger drop diameters and high oil concentration that are to be expected there.

As an alternative, video imaging systems can be used for droplet size measurements. A promising approach by Davies et al. (2017) uses a holographic camera system to size particles in sample volume with 3–50 mm path length. The large path length and adjustable magnification enable sizing in the range of 28  $\mu\text{m}$  to several millimetres. Based on backlighted images of small sample volumes, oil concentration is again a limiting factor in this approach as images should ideally contain no overlapping particles in the view plane to enable automated image analysis and sizing. In addition, a narrow path length and small sample volume poses the risk of under-sampling large particles (Davies et al. 2017).

At the cost of generating images that might not be automatically evaluable, endoscopic systems with incident lighting can handle very high oil concentrations over a large diameter range in the order of magnitude from  $10^1$  to  $10^3$   $\mu\text{m}$  (Maaß et al. 2011; Malone et al. 2018).

#### 4.2.5 Critical Review of Datasets

The confident translation of laboratory or pilot-scale experiments to the field remains an outstanding research objective. Multiple authors have proposed correlations with the claim of accurately representing the field scale, yet in all cases the empirical or semiempirical correlations employed require *extrapolation*. Fundamentally, the scientific method imposes an upper limit on the confidence of any extrapolation, particularly in the case it includes any empirical contribution. While several scaling quantities may be considered to unite laboratory and pilot-scale data, including the Reynolds and Weber numbers, it should be recognized that these quantities are fundamentally *approximations* that balance contributions in *simple* turbulent systems. To be clear, the Weber and Reynolds numbers *are not defined for a turbulent plume and are not defined for a flow system containing dispersed phases (oil, gas and potentially hydrate in this case)*. As a consequence, the attempts to unify the datasets reported in Table 4.1 within a single correlation have failed to date. One attempt has shown limited success – as discussed in Sect. 4.3.3 – where turbulence is evaluated at a more *fundamental* level than the Weber and Reynolds numbers provide.

### 4.3 Modelling Approaches

Based on the experimental and field data presented in the previous section and Table 4.1, different models were developed to predict the initial droplet size distribution of an accidental subsea oil discharge. These models can be divided into two



**Table 4.1** Experimental measurements of oil droplet size distributions

Study	DeepSpill (Johansen et al. 2000)	Masutani and Adams (2001)	Brandvik et al. (2013)	Belore (2014)	Aman et al. (2015)	Zhao et al. (2016)	Brandvik et al. (2017)	Malone et al. (2018)
No. of datasets (no. of dispersant cases thereof)	1	71	15 (8)	56 (56)	8	1	24 (12)	8
Varied parameter(s)	–	Oil type, Q, D	Q, D, DOR	Oil type, Q, D, GOR, DOR	Turning speed	–	Gas void fraction, DOR, p, T	Gas saturation, oil type, Q
Oil type(s)	Marine diesel fuel	4 crudes, silicone oil	Oseberg blend	Endicott crude, dorado crude	Louisiana sweet crude	JP 5 (jet fuel oil)	Oseberg blend	Louisiana sweet crude, n-decane
Hydrostatic pressure	85 atm	1 atm	1.6 atm	1 atm	110 atm	1 atm	59–172 bar	151 atm
Gas-saturated oil?	No	No	No	No	Yes	No	Yes	Yes, partly
Gas void fraction	Yes	No	Partly	Yes	No	No	Yes, partly	No
Nozzle diameter	120 mm	1 mm; 2 mm; 5 mm	0.5 to 3 mm	1.5 mm; 4.5 mm	n/a	25.4 mm	3 mm	1.5 mm
Oil volume flow	60 m <sup>3</sup> /h	0.05 to 3 L/min	0.2 to 5 L/min	0.285 to 1.5 L/min	n/a	378 L/min	1.5 L/min	1.1–2.1 L/min
Dispersant	No	No	Yes, partly	Yes, all	No	No	Yes, partly	No
Reynolds number (only no dispersant cases)	Approx. 3.9*10 <sup>4</sup>	23 to 795	1.4–8.9*10 <sup>3</sup>	n/a	1.1–5.4*10 <sup>3</sup>	5.9*10 <sup>4</sup>	8.4–9.7 *10 <sup>3</sup>	0.16–3.0*10 <sup>4</sup>
Weber number (only no dispersant cases)	Approx. 2.5*10 <sup>4</sup>	40 to 1860	0.7–7.6*10 <sup>4</sup>	n/a	50–300	1.6*10 <sup>5</sup>	1.3–1.5*10 <sup>3</sup>	0.22–2.2*10 <sup>4</sup>

principal groups: models that use characteristic flow parameters for up- or down-scaling of a median diameter and models that calculate a complete droplet size distribution through mechanistic modelling of the flow. Both groups differ widely with regard to the computational effort but also with regard to the level of detail of the result.

### 4.3.1 Scaling-Based Models Using Dimensionless Numbers

Probably the most widely used scaling approach in the oil spill community is the modified Weber number scaling by Johansen et al. (2013). Based on the model of Wang and Calabrese (1986) for stirred-tank reactors, they proposed the implicit scaling law for the volume median diameter  $d_{v50}$

$$\frac{d_{v50}}{D} = A \cdot \text{We}^{*-3/5} \quad (4.7)$$

with the modified Weber number  $\text{We}^*$

$$\text{We}^* = \frac{\text{We}}{\left[ 1 + B \cdot \text{Vi} \cdot \left( \frac{d_{v50}}{D} \right)^{\frac{1}{3}} \right]} \quad (4.8)$$

where  $\text{We} = \frac{D \cdot \rho_1 \cdot u_1^2}{\sigma_1}$  is the Weber number,  $\text{Vi} = \frac{\text{We}}{\text{Re}}$  the viscosity number and  $A$  and  $B$  are empirical coefficients. Those coefficients were calculated using the dataset of Brandvik et al. (2013) to be  $A = 15$  and  $B = 0.8$ ; a later work based on a larger dataset updates these to  $A = 24.8$  and  $B = 0.08$  (Socolofsky et al. 2015). The data used to calibrate the model span a range of approximately  $10^3 \leq \text{We} \leq 10^4$  and jets with and without additional dispersant injection. The authors claim the model to be applicable to multiphase discharges of oil and gas as well by adjusting the exit velocity  $u_1$  to account for the gas phase and its buoyancy.

A second model, called the unified droplet size model, by Li et al. (2017) scales the volume median diameter  $d_{v50}$  with a combination of Weber and Ohnesorge number in an explicit equation:

$$\frac{d_{v50}}{D} = r \cdot (1 + 10 \cdot \text{Oh})^p \cdot \text{We}^q \quad (4.9)$$

where  $r = 14.05$ ,  $p = 0.460$  and  $q = -0.518$  are empirically derived coefficients for a liquid-liquid jet. The model is proposed for determining both the  $d_{v50}$  of a jet and of wave entrainment at the surface. The coefficients  $p$  and  $q$  were determined based

on 28 wave entrainment datasets, whereas  $r$  was calculated from the  $d_{v50}$  of the Norwegian DeepSpill experiment. The model was tested against both laboratory data and field measurements by a Holocam during the DWH spill (Li et al. 2015).

Both models provide a median volume diameter at very little computational cost. As input parameters, both require the same information about the physical properties of the oil, oil exit velocity and exit diameter. Especially with regard to the physical properties of “live” oil under deep-sea conditions (high pressure, low temperature), there are often no measured data, and the properties can only be calculated using empirical correlations (Lake and Fanchi 2006) or numerical models (Gros et al. 2016). In addition, they have only been validated for “dead oil” in a limited range of  $We$  and  $Oh$  and require extrapolation over several orders of magnitude beyond these limits to provide an estimation for a major spill like DWH.

The scaling laws described above only provide a steady-state volume median diameter and no actual size distribution. However, as the size distribution may differ widely for different blowout scenarios (Malone et al. 2018), information on the spreading factor of the underlying distribution factor is of considerable importance for a realistic near- and far-field modelling (see Vaz et al. 2020; Perlin et al. 2020).

### 4.3.2 Mechanistic Modelling

A different approach by Zhao et al. (2014, 2017) uses a hydrodynamic model of the jet to predict the complete drop size distribution. The Lagrangian model, called VDROD-J, calculates the DSD of a small portion of the jet based on a population balance of drop breakup and coalescence in a given time step. A single large drop size is taken as initial input and tracked downstream while the jet widens and takes in water, thereby reducing the oil fraction in the considered portion of the jet. Breakage rate is determined stepwise by the probability of a drop to collide with a turbulent eddy with sufficient energy to cause breakup of this drop; coalescence rate is defined by the probability of two drops colliding and coalescing due to turbulence.

As an outcome, this model provides the full DSD of a jet at different positions downstream of the orifice, albeit at significant computational cost. Because the DSD is directly calculated from the discharge conditions without the need for upscaling by several orders of magnitude, it is less sensitive to miscorrelation of experimental data than scaling-based models. However, a crucial point in the calculation of the DSD is turbulent dissipation rate in the jet, which can be seriously affected by reactions and interactions of the multiphase flow of oil, gas, water and possibly hydrates that are discharged in a major subsea spill like DWH, and which are not yet fully understood.

### 4.3.3 *Novel Applications of Energy Dissipation Metrics to Understand Droplet Sizes from Experimental Data*

To date, the prediction of live oil droplet size distributions has been treated with two approaches: (i) the use of a modified Weber number scaling, proposed by Johansen et al. (2013), and (ii) the use of Reynolds number, proposed by Aman et al. (2015). In *both* cases, the studies define their respective dimensionless quantities based on the physical conditions at the contact point of the blowout preventer (BOP) stack and the seawater; that is, the internal *oil pipe diameter* was employed as the singular property to define the length scale of the problem. This understanding clarifies why both methods have failed to unify the available data: oil droplets are not created at the exit point of the pipe, but rather in the near-field plume. As such, the research community must understand and characterize turbulence *at the point of droplet creation* using a more fundamental basis of turbulence that can incorporate the *known* contributions.

One such approach may be derived by evaluating both the turbulent kinetic energy (TKE) and turbulence dissipation rate (TDR), which, respectively, describe the energetic content of the eddies in the flow and the rate at which eddies transfer TKE down the so-called energy cascade. As droplets are generated through the *transfer* of TKE, the use of TDR-based scaling provides an attractive opportunity to compare the available datasets. To this end, models must consider the three relevant contributions to TDR in the context of a subsea blowout: (i) the momentum of the gas/oil jet itself, defined between the exit of the pipe and the top of the near-field plume; (ii) the additional momentum generated *inside* the BOP stack, where fluids experienced an 84-bar orifice pressure drop imposed by the annular preventer within a few diameters of the exit point; and (iii) additional turbulence introduced by the evolution of free gas from live oil droplets. To date, computational fluid dynamics (CFD) approaches have been unable to rationalize all three contributions together. However, the first two contributions may be estimated from experimental laboratory studies, to estimate the range of probable TDR in the field case.

Zhao et al. (2014) summarized experimental TDR estimates for *single-phase jets* (the first contribution above), deriving a correlation as a function of jet exit diameter, velocity and distance into the plume. The study demonstrated that, within 10 diameters of the exit, the TDR remains constant and decreases monotonically thereafter; as such, the maximum TDR corresponding to the jet momentum may be conservatively estimated. This TDR method can be applied to data collected on the apparatus at SINTEF, SWRI and TUHH (as described above). Through the use of CFD to map stirred cells, Booth et al. (2018) have further demonstrated the ability to correlate TDR for autoclave systems employed at the University of Western Australia. For the range of volumetric flowrates reported in the DWH blowout and for the relevant range of oil and gas properties, the TDR correlation from Zhao et al. (2014) suggests a TDR range of between  $10^{-3}$  and  $10^{-5}$   $\text{m}^2 \text{s}^{-3}$ , which only represents the first contribution identified above. For reference, most autoclave

experiments are performed between  $10^{-2}$  and  $10^2 \text{ m}^2 \text{ s}^{-3}$ , while most data from pilot-scale jets corresponds to TDRs between  $10^3$  and  $10^5 \text{ m}^2 \text{ s}^{-3}$ .

The DWH jet was also influenced by a partially closed annular preventer, which closely resembles a classical orifice and imposed an 84-bar pressure drop within a few diameters of the exit point. This contribution of this orifice drop to the TDR has largely been neglected to date. Kundu et al. (2016) provide a well-established relation from fluid mechanics to estimate TDR contribution from a restricted pressure drop:

$$\varepsilon_{\text{pd}} = \frac{\Delta p \cdot Q}{\rho_c \cdot V} \quad (4.10)$$

where  $\Delta p$  is the permanent pressure drop applied by the restriction,  $Q$  is the volumetric flowrate through the restriction,  $\rho_c$  is the continuous phase density and  $V$  is the volume of energy dissipation (e.g. the volume of the BOP stack). With an 84-bar pressure drop, an average fluid density of  $700 \text{ kg/m}^3$  and a 2 m height of the BOP stack with a 0.5 m internal diameter, this orifice contribution to TDR is estimated at  $2700 \text{ m}^2 \text{ s}^{-3}$ .

The third contribution above – from live oil degassing – has not been studied in sufficient detail to quantitatively inform contributions to TDR. However, the first two contributions identified above demonstrate the elegant rationale as to why Weber- and Reynolds-based scaling arguments have failed to unify the available data: such approaches *severely underrepresent the turbulence of the Macondo plume, because they only account for the first of two important contributions*. That is, the TDR contribution from the orifice pressure drop aligns well with the magnitude of TDRs captured at high mixing speed in autoclaves or in most pilot-scale jet experiments. Importantly, neither Weber- nor Reynolds-based methods are *able* to capture the additional TDR contributions from the orifice pressure drop, resulting in the discrepancy of predicted droplet sizes heretofore.

#### 4.4 Effects of Deep-Sea Blowout Characteristics

In case of a large-scale, deep-sea oil discharge from an uncontrolled well, several factors must be considered in addition to the modelling approaches presented in Sect. 4.3. These are mainly:

- Gaseous components ( $\text{C}_1\text{-C}_5$ ,  $\text{N}_2$ ,  $\text{CO}_2$ ,  $\text{H}_2\text{S}$ ) dissolved in the crude oil (“live” instead of “dead” oil).
- A multiphase flow (oil, gas, water) inside the borehole and at the wellhead.
- High hydrostatic pressure and low temperature of the surrounding seawater.
- Rapid pressure and temperature changes at the wellhead, inducing phase changes in the oil.

For the DWH spill, the fluid exiting the wellhead consisted of approx. 40–50 vol% gaseous components (mainly methane) and 50–60 vol% oil, which was by itself saturated with dissolved gases (Reddy et al. 2012; Boufadel et al. 2018). The fluid experienced a pressure drop of approximately 86 bar (Lehr et al. 2010) within the BOP and cooled from approximately 105 to 4.3 °C within a few meters distance from the discharge point (Reddy et al. 2012; Gros et al. 2016).

#### ***4.4.1 Influence of Dissolved Gases on the Droplet Size Distribution***

As the solubility of many gases in oil rises linearly with pressure (Jaggi et al. 2017), the amount of short-chained hydrocarbons such as  $C_1$  to  $C_5$  dissolved in crude oil can be hundredfold at reservoir or deep-sea conditions compared to sea surface conditions (Lehr and Socolofsky 2020). For the DWH spill, Gros et al. (2016) calculated the amount of methane dissolved to be 141 times higher at the wellhead than at the sea surface. A crude oil with such an amount of dissolved and volatile components, such as it exists inside the reservoir itself, is commonly called a “live oil”, in comparison to a “dead oil” at ambient conditions with no or just very little dissolved gases (Ahmed 2010). While “dead” oil is a nearly incompressible liquid and is comparatively unaffected by an elevated hydrostatic pressure, the properties of “live oil” will change significantly with increasing pressure due to the increased amount of dissolved gas. For more details on the effect of deep-sea conditions on physical and chemical properties of oil and gas, please see Oldenburg et al. (2020).

Two recent studies performed by SINTEF and Hamburg University of Technology investigated the effect of dissolved gas on the DSD of a crude oil under elevated hydrostatic pressure (Brandvik et al. 2017; Malone et al. 2018). As Brandvik et al. (2017) also reported the formation of gas bubbles in their experiments, the “live oil” must have undergone a phase change during the discharge, which means that the results cannot be attributed to the “live oil” properties only. They do, however, report an underestimation of volume median diameter by the modified We-scaling model by approximately 10%.

At Hamburg University of Technology, a direct comparison between two “dead” and “live” oils (Louisiana sweet crude oil and n-decane) was performed using the same setup and experimental conditions (Malone et al. 2018). Oil jets were generated quasi-isobaric by using an equal-volume cylinder in order to exclude any side effects of a pressure change on the oil (Seemann et al. 2014, Malone et al. 2018). Median diameters of “live oil” were increased by 74% to 97% compared to “dead oil” under otherwise unchanged conditions. The experimental data was compared with the models by Johansen and Li (Johansen et al. 2013, Li et al. 2017), which account for changes of the physical properties density, viscosity and IFT by use of the dimensionless numbers We and Re (see Sect. 4.3.1). Both models predicted a very similar  $d_{v,50}$  for “live” and “dead” oil in contrast to the experimental results.

A possible explanation for this unexpected size increase could be the increased compressibility of the “live oil” (Satter and Iqbal 2016) which would reduce the TKE of the jet by elastic deformation of individual drops rather than breakup.

In addition, the size distribution of the “live oil” was significantly broader compared to the dead oil. While both “live” and “dead” oil discharges followed a log-normal distribution function, the spreading factor  $\sigma$  varied widely for the different oils and increased from “dead” to “live” oil by over 30%.

#### ***4.4.2 Influence of Rapid Pressure Loss at the Wellhead and Phase Changes of the Oil***

According to Lehr et al. (2010), the pressure of the oil at the DWH spill site changed rapidly from 241 bar measured inside the BOP to 154 bar ambient hydrostatic pressure after exiting the wellhead. This change took place over a height of only 16.4 m. As a result from this rapid pressure loss and the previous, slow decompression along the borehole, a multiphase flow of “live oil” and gas is discharged from the wellhead. Due to the pressure-dependent solubility of gaseous components in the crude oil (Chap. 3 and Sect. 4.4.1), such a massive pressure drop can lead to an oversaturation of the oil and therefore outgassing of  $C_1$  to  $C_5$  in addition to the expansion of the already existing gas phase. This outgassing and gas expansion might affect the drop formation in different ways. First, the expansion of a separate gas phase will add to the overall TKE of the multiphase plume by its expansion energy. Secondly, outgassing from the oversaturated oil will lead to the formation of a gas phase within the oil drops, which will significantly alter and destabilize the drop. The gas microbubbles might either leave the oil drop at its surface, thereby removing parts of the oil from the “mother drop” or expand within the drop, thereby forming a two-phase particle with different breakup and rising characteristics (see also Pesch et al. 2020 on the rise velocity of live oil droplets). Both effects are depicted in Fig. 4.2.

To assess the effect of such a pressure drop on the DSD, oil jets of both “live” and “dead” oil were generated at Hamburg University of Technology with a defined pressure difference between oil reservoir pressure and hydrostatic pressure of the seawater. For this purpose, a throttle valve was added in front of the nozzle of the experimental setup described in Seemann et al. (2014) and Malone et al. (2018) to generate the required pressure drop. The oil reservoir was pressurized to 161 bar, while the seawater basin was kept at 151 bar pressure like in the earlier experiments. The DSD was determined from manually evaluated images of an endoscopic camera system (Malone et al. 2018).

With this pressure drop of  $\Delta p = 10$  bar, the “dead oil” droplet sizes were distributed log-normally as expected, whereas the “live oil” was distributed bimodally. This bimodal distribution could very well be described by superposing two log-normal distributions. It is assumed that this bimodality is caused by the processes hypothesized above and depicted in Fig. 4.2. Under this assumption, the larger



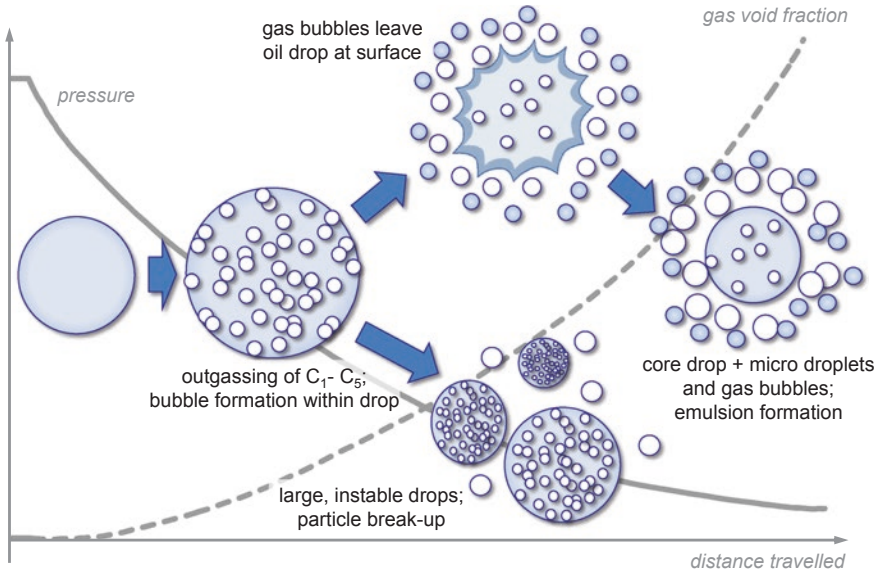


**Fig. 4.2** Possible effects of oversaturation and outgassing on the drop formation and drop size distribution after a rapid pressure drop (not to scale)

mode is formed by those drops where no or very few gas bubbles nucleated. The smaller mode consists of drops that were split up when the gas bubbles nucleated, expanded and exited the oil drop. That gas bubbles did in fact form and expand prior to the measurement point is evident from the footage of the surveillance camera (Fig. 4.3), though those bubbles were not captured by the measurement system in sufficient numbers to allow for quantification. This interpretation of the bimodality is supported when plotting the median volume diameter of both modes over the modified Weber number (Fig. 4.4). While the  $d_{v50}$  of the larger mode lies in approximately the same range as the quasi-isobaric live oil from Malone et al. (2018) and is significantly enhanced compared to the “dead” oil and the model prediction by Johansen et al. (2013), the  $d_{v50}$  of the smaller mode is significantly smaller than either the “live” or the “dead oil”. In terms of the TKE, the pressure drop from the oil reservoir and subsequent outgassing of methane from the oil provide an additional energy source in the jet leading to further breakup of the oil droplet and consequently a smaller median drop diameter.

Plotting the volume median diameters from both the quasi-isobaric and the “pressure drop” experiments at Hamburg University of Technology over the maximum TKE according to Zhao et al. (2014)

$$\varepsilon_u = 0.003 \cdot u_1^3 / D \quad (4.11)$$

reveals the good correlation of the different data sets to the assumptions on the effects of gas dissolution and pressure drop/outgassing (Fig. 4.5).



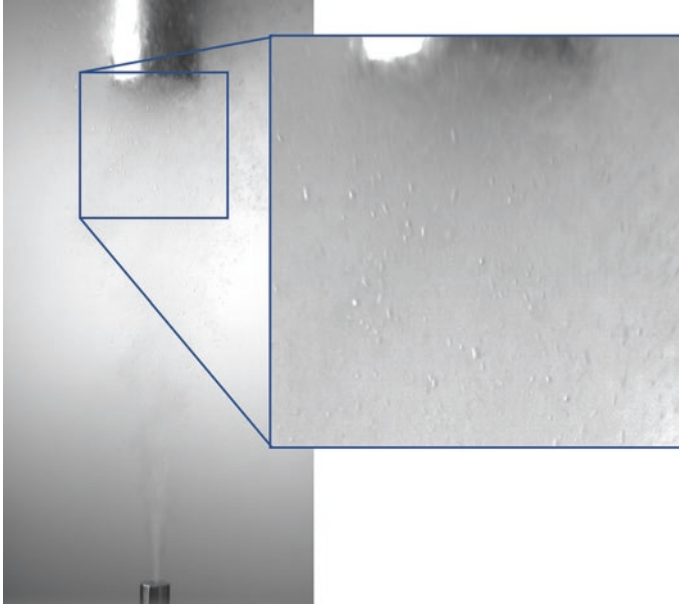


**Fig. 4.3** Methane-saturated n-decane discharged into artificial seawater at 150 bar ambient pressure, 20 °C. Methane bubbles form from the oversaturated n-decane after a pressure drop of 10 bar from the oil reservoir

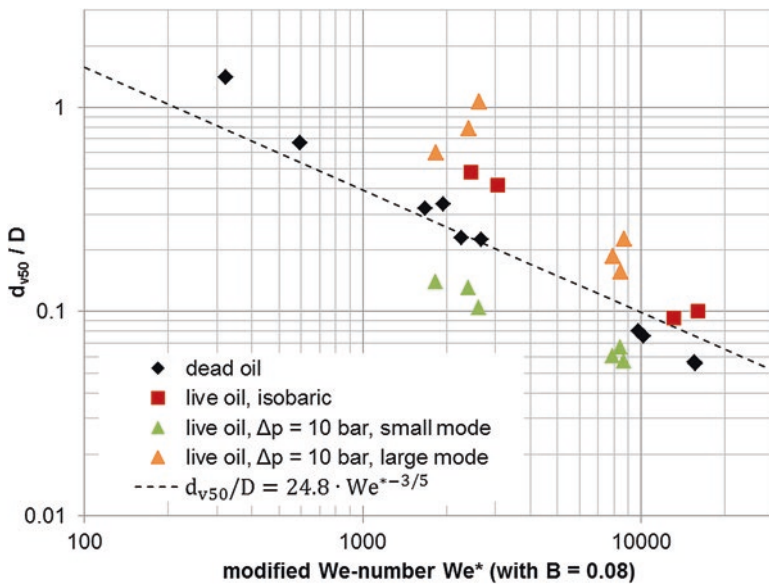


**Fig. 4.4** Comparison of experimental result from jet experiments at Hamburg University of Technology to  $We^*$ -scaling model proposed by Johansen et al. (2013)

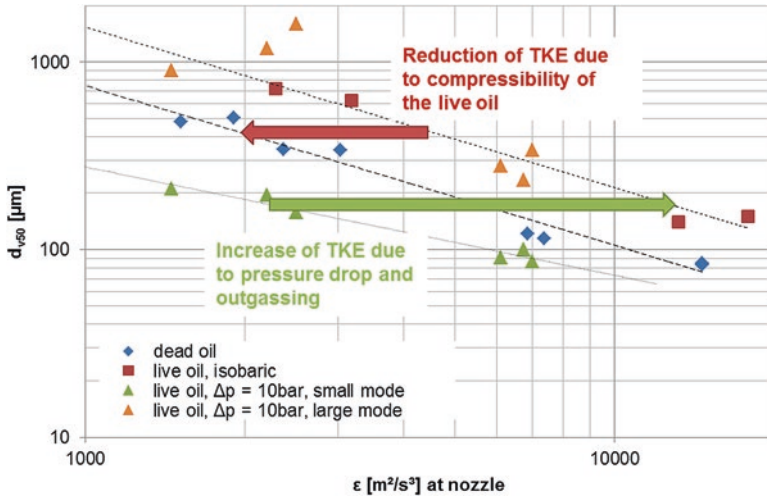


**Fig. 4.5** Effects of deep-sea oil characteristics on the volume median diameter and the maximum turbulent kinetic energy. Dashed lines are provided to guide the eye

## 4.5 Capabilities and Limits of Subsea Dispersant Injection

The above-referenced autoclave and pilot-scale jet studies have also considered the effect of dispersant injection, typically at dispersant-to-oil ratios of between 1:100 and 1:20. Interestingly, the results demonstrate minimal dependence between the reported average droplet size and the maximum TDR in any system, including wave tank studies from the EPA (Fig. 4.6). Within the context of the estimated TDR contributions for Macondo, the data show that oil droplet sizes are similar with and without dispersant application. Further studies across multiple mixing geometries, DORs and gas/oil properties are required to fully contextualize the critical TDR range under which dispersant application may benefit droplet size.

## 4.6 Conclusions and Outlooks

The determination of the initial size distribution of oil drops and gas bubbles is still a major challenge in modelling of deep-sea oil spills.

The state-of-the-art knowledge on drop formation is mainly based on small-scale lab experiments of liquid-liquid jets at ambient conditions. For a better understanding of future oil spills, investigations at deep-sea conditions as well as in situ measurements with capable equipment are critical. Despite numerous attempts, a reliable translation of laboratory or pilot-scale experiments to the field conditions including a turbulent, multiphase plume remains an outstanding research objective.

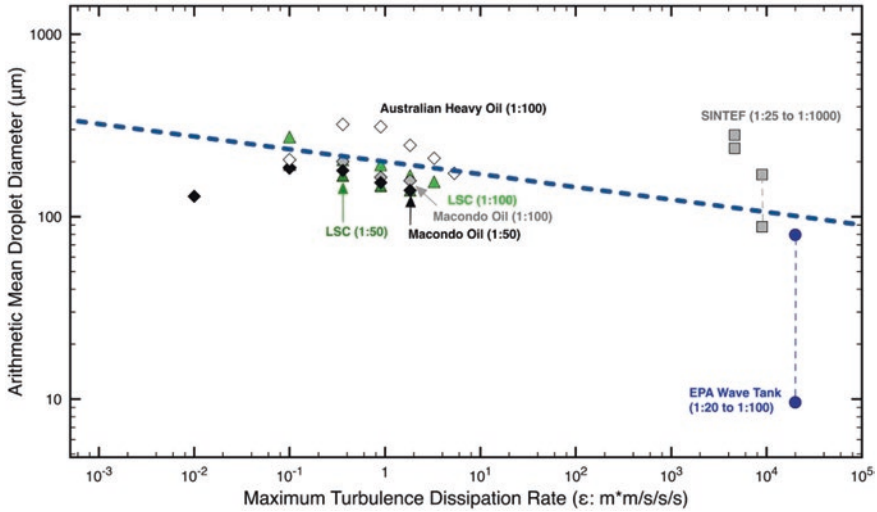


**Fig. 4.6** Average reported droplet size as a function of maximum TDR for sapphire autoclave measurements (left-hand grouping), wave tank studies (blue circles) and pilot-scale blowout jets (grey squares) containing dispersant; DORs relative to each study are shown in parentheses. The dashed line is provided to guide the eye

A new approach to predict the median drop diameter based on the turbulent energy dissipation rate was presented in this chapter. To be able to generalize this approach, further studies across multiple mixing geometries, DORs and gas/oil properties are required.

Recent studies at artificial deep-sea conditions at Hamburg University of Technology showed a significant influence of dissolved gases and outgassing on the drop size distribution. In a first attempt, these influences could be modelled with good accuracy using the turbulent energy dissipation rate. Especially the outgassing of short-chained hydrocarbons from the oil might lead to a significant decrease in the median drop diameter, as oil drops are broken up by expanding gas bubbles.

To be better prepared for a possible future spill in the deep-sea, it is necessary to investigate the high-pressure, multiphase plume near the exit at a more detailed level and at a larger scale than heretofore. Only by a thorough understanding of the drop formation processes and turbulent conditions in this multiphase plume is it possible to find a knowledge-based mitigation strategy, which might or might not include subsea dispersant injection.

**Acknowledgments** This research was made possible by a grant from the Gulf of Mexico Research Initiative/C-IMAGE. Data are publicly available through the Gulf of Mexico Research Initiative Information and Data Cooperative (GRIIDC) at <https://data.gulfresearchinitiative.org/> (DOIs: 10.7266/n7-jjqd-pa77, 10.7266/n7-eha7-tv03, 10.7266/N7V69H19, 10.7266/N77D2SM2).

## References

- Adams EE, Socolofsky SA (2004) Review of deep oil spill modeling activity supported by the DeepSpill JIP and offshore operators committee: Final Report. 26 pp
- Ahmed TH (2010) Reservoir engineering handbook, 4th edn. Gulf Professional, Oxford
- Aman ZM, Paris CB, May EF, Johns ML, Lindo-Atichati D (2015) High-pressure visual experimental studies of oil-in-water dispersion droplet size. *Chem Eng Sci* 127:392–400. <https://doi.org/10.1016/j.ces.2015.01.058>
- Belore R (2014) Subsea chemical dispersant research. In: Proceedings of the 37th AMOP technical seminar on environmental contamination and response, Canmore, Alberta
- Booth CP, Leggoe JW, Aman ZM (2018) The use of computational fluid dynamics to predict the turbulent dissipation rate and droplet size in a stirred autoclave. *Chem Eng Sci*. In Press
- Boufadel MC, Gao F, Zhao L, Özgökmen T, Miller R, King T, Robinson B, Lee K, Leifer I (2018) Was the Deepwater Horizon well discharge churn flow?: implications on the estimation of the oil discharge and droplet size distribution. *Geophys Res Lett* 45:2396–2403. <https://doi.org/10.1002/2017GL076606>
- Boxall JA, Koh CA, Sloan ED, Sum AK, Wu DT (2012) Droplet size scaling of water-in-oil emulsions under turbulent flow. *Langmuir* 28:104–110. <https://doi.org/10.1021/la202293t>
- Brandvik PJ, Johansen Ø, Leirvik F, Farooq U, Daling PS (2013) Droplet breakup in subsurface oil releases – part 1: Experimental study of droplet breakup and effectiveness of dispersant injection. *Mar Pollut Bull* 73:319–326. <https://doi.org/10.1016/j.marpolbul.2013.05.020>
- Brandvik PJ, Davies EJ, Storey C, Leirvik F, Krause DF (2017) Subsurface oil releases – verification of dispersant effectiveness under high pressure using combined releases of live oil and natural gas, SINTEF report no: A27469. Trondheim Norway 2016. ISBN: 978-821405857-4
- Davies EJ, Brandvik PJ, Leirvik F, Nepstad R (2017) The use of wide-band transmittance imaging to size and classify suspended particulate matter in seawater. *Mar Pollut Bull* 115:105–114. <https://doi.org/10.1016/j.marpolbul.2016.11.063>
- Gros J, Reddy CM, Nelson RK, Socolofsky SA, Arey JS (2016) Simulating gas–liquid–water partitioning and fluid properties of petroleum under pressure: implications for deep-sea blowouts. *Environ Sci Technol* 50:7397–7408. <https://doi.org/10.1021/acs.est.5b04617>
- Hsiang L-P, Faeth GM (1992) Near-limit drop deformation and secondary breakup. *Int J Multiphase Flow* 18:635–652
- Jaggi A, Snowdon RW, Stopford A, Radović JR, Oldenburg TB, Larter SR (2017) Experimental simulation of crude oil-water partitioning behavior of BTEX compounds during a deep submarine oil spill. *Org Geochem* 108:1–8. <https://doi.org/10.1016/j.orggeochem.2017.03.006>
- Johansen Ø, Rye H, Melbye AG, Jensen HV, Serigstad B, Knutsen T (2000) Deep spill JIP - experimental discharges of gas and oil at Helland Hansen – June 2000, Technical Report
- Johansen Ø, Brandvik PJ, Farooq U (2013) Droplet breakup in subsea oil releases--part 2: Predictions of droplet size distributions with and without injection of chemical dispersants. *Mar Pollut Bull* 73:327–335. <https://doi.org/10.1016/j.marpolbul.2013.04.012>
- Kundu PK, Cohen IM, Dowling DR (2016) Fluid mechanics, Sixth edition. Academic Press, Oxford
- Lake LW, Fanchi JR (2006) Petroleum engineering handbook. Society of Petroleum Engineers, Richardson
- Lefebvre AH, McDonnell VG (2017) Atomization and sprays, Second edition. CRC Press, Boca Raton
- Lehr W, Socolofsky SA (2020) The importance of understanding fundamental physics and chemistry of deep oil blowouts (Chap. 2). In: Murawski SA, Ainsworth C, Gilbert S, Hollander D, Paris CB, Schlüter M, Wetzel D (eds) Deep oil spills: facts, fate, effects. Springer, Cham
- Lehr B, Aliseda A, Bommer P, Espina P, Flores O, Lasheras JC, Leifer I, Possolo A, Riley J, Savas O, Shaffer F, Wereley S, Yapa PD (2010) Deepwater Horizon Release: estimate of rate by PIV, July 21, 2010, Accessed on October 29, 2018. <https://www.doi.gov/sites/doi.gov/files/migrated/>

[deepwaterhorizon/upload/Deepwater\\_Horizon\\_Plume\\_Team\\_Final\\_Report\\_7-21-2010\\_comp-corrected2.pdf](#)

- Li Z, Bird A, Payne JR, Vinhateiro N, Kim Y, Davis C, Loomis N (2015) Technical reports for Deepwater Horizon water column injury assessment: oil particle data from the Deepwater Horizon oil spill. <https://www.fws.gov/doiddata/dwh-ar-documents/946/DWH-AR0024715.pdf>. Accessed 28 Sept 2018
- Li Z, Spaulding M, French McCay D, Crowley D, Payne JR (2017) Development of a unified oil droplet size distribution model with application to surface breaking waves and subsea blowout releases considering dispersant effects. *Mar Pollut Bull* 114:247–257. <https://doi.org/10.1016/j.marpolbul.2016.09.008>
- Maaß S, Wollny S, Voigt A, Kraume M (2011) Experimental comparison of measurement techniques for drop size distributions in liquid/liquid dispersions. *Exp Fluids* 50:259–269. <https://doi.org/10.1007/s00348-010-0918-9>
- Malone K, Pesch S, Schlüter M, Krause D (2018) Oil droplet size distributions in deep-sea blowouts: influence of pressure and dissolved gases. *Environ Sci Technol* 52:6326–6333. <https://doi.org/10.1021/acs.est.8b00587>
- Masutani S, Adams EE (2001) Experimental study of multiphase plumes with application to deep ocean oil spills: final report to U.S. Dept. of the Interior
- Ohnesorge WV (1936) Die Bildung von Tropfen an Düsen und die Auflösung flüssiger Strahlen. *Z Angew Math Mech* 16:355–358. <https://doi.org/10.1002/zamm.19360160611>
- Oldenburg TBP, Jaeger P, Gros J, Socolofsky SA, Pesch S, Radović J, Jaggi A (2020) Physical and chemical properties of oil and gas under reservoir and deep-sea conditions (Chap. 3). In: Murawski SA, Ainsworth C, Gilbert S, Hollander D, Paris CB, Schlüter M, Wetzel D (eds) *Deep oil spills: facts, fate, effects*. Springer, Cham
- Perlin N, Paris CB, Berenshtein I, Vaz AC, Failetta R, Aman ZM, Schwing PT, Romero IC, Schlüter M, Liese A, Noirungsee N, Hackbusch S (2020) Far-field modeling of a deep-sea blowout: sensitivity studies of initial conditions, bio-degradation, sedimentation and sub-surface dispersant injection on surface slicks and oil plume concentrations (Chap. 11). In: Murawski SA, Ainsworth C, Gilbert S, Hollander D, Paris CB, Schlüter M, Wetzel D (eds) *Deep oil spills: facts, fate, effects*. Springer, Cham
- Pesch S, Schlüter M, Aman ZM, Malone K, Krause D, Paris CB (2020) Behavior of rising droplets and bubbles – impact on the physics of deep-sea blowouts and oil fate (Chap. 5). In: Murawski SA, Ainsworth C, Gilbert S, Hollander D, Paris CB, Schlüter M, Wetzel D (eds) *Deep oil spills: facts, fate, effects*. Springer, Cham
- Reddy CM, Arey JS, Seewald JS, Sylva SP, Lemkau KL, Nelson RK, Carmichael CA, McIntyre CP, Fenwick J, Ventura GT, van Mooy BAS, Camilli R (2012) Composition and fate of gas and oil released to the water column during the Deepwater Horizon oil spill. *Proc Natl Acad Sci* 109:20229–20,234. <https://doi.org/10.1073/pnas.1101242108>
- Satter A, Iqbal GM (2016) *Reservoir engineering: the fundamentals, simulation, and management of conventional and unconventional recoveries*. Elsevier/Gulf Professional Publishing, Amsterdam
- Seemann R, Malone K, Laqua K, Schmidt J, Meyer A, Krause D, Schlüter M (2014) A new high-pressure laboratory setup for the investigation of deep-sea oil spill scenarios under in-situ conditions. In: *Proceedings of the seventh International Symposium on Environmental Hydraulics*, pp 340–343
- Socolofsky SA, Adams EE, Boufadel MC, Aman ZM, Johansen Ø, Konkel WJ, Lindo D, Madsen MN, North EW, Paris CB, Rasmussen D, Reed M, Rønningen P, Sim LH, Uhrenholdt T, Anderson KG, Cooper C, Nedwed TJ (2015) Intercomparison of oil spill prediction models for accidental blowout scenarios with and without subsea chemical dispersant injection. *Mar Pollut Bull* 96:110–126. <https://doi.org/10.1016/j.marpolbul.2015.05.039>
- Tang L (2004) *Cylindrical liquid-liquid jet instability*. Ph. D. Thesis
- Vaz AC, Paris CB, Dissanayake AL, Socolofsky SA, Gros J, Boufadel MC (2020) Dynamic coupling of near-field and far-field models (Chap. 9). In: Murawski SA, Ainsworth C, Gilbert S, Hollander D, Paris CB, Schlüter M, Wetzel D (eds) *Deep oil spills: facts, fate, effects*. Springer, Cham

- Wang CY, Calabrese RV (1986) Drop breakup in turbulent stirred-tank contactors. Part II: relative influence of viscosity and interfacial tension. *Am Inst Chem Eng J* 32:667–676. <https://doi.org/10.1002/aic.690320417>
- Zhao L, Boufadel MC, Socolofsky SA, Adams E, King T, Lee K (2014) Evolution of droplets in sub-sea oil and gas blowouts: development and validation of the numerical model VDROD. *J. Mar Pollut Bull* 83:58–69. <https://doi.org/10.1016/j.marpolbul.2014.04.020>
- Zhao L, Shaffer F, Robinson B, King T, D'Ambrose C, Pan Z, Gao F, Miller RS, Conmy RN, Boufadel MC (2016) Underwater oil jet: hydrodynamics and droplet size distribution. *Chem Eng J* 299:292–303. <https://doi.org/10.1016/j.cej.2016.04.061>
- Zuzio D, Estivaleres J-L, Villedieu P, Blanchard G (2013) Numerical simulation of primary and secondary atomization. *Comptes Rendus Mécanique* 341:15–25. <https://doi.org/10.1016/j.crme.2012.10.003>